JOURNAL OF APPLIED CRYSTALLOGRAPHY

ISSN: 1600-5767

journals.iucr.org/j

A-site order in rhombohedral perovskite-like oxides $La_{2-x}Sr_xCoTiO_6$ ($0.6 \leq x \leq 1.0$)

Alejandro Gómez-Pérez, Clemens Ritter, Khalid Boulahya, Alvaro Muñoz-Noval, Flaviano García-Alvarado and Ulises Amador

J. Appl. Cryst. (2016). **49**, 31–39

JOURNAL OF APPLIED CRYSTALLOGRAPHY

ISSN 1600-5767

Received 27 April 2015
Accepted 25 November 2015

Edited by D. Pandey, Indian Institute of Technology (Banaras Hindu University), Varanasi, India

Keywords: perovskites; phase transitions; neutron diffraction; synchrotron X-ray diffraction; *AMPLIMODES*; cobaltite.

Supporting information: this article has supporting information at journals.iucr.org/j

A-site order in rhombohedral perovskite-like oxides $La_{2-x}Sr_xCoTiO_6$ ($0.6 \leq x \leq 1.0$)

Alejandro Gómez-Pérez,[a]* Clemens Ritter,[b] Khalid Boulahya,[c] Alvaro Muñoz-Noval,[d,e] Flaviano García-Alvarado[a] and Ulises Amador[a]*

[a]Quimica Facultad de Farmacia, Universidad CEU-San Pablo, Carretera de Boadilla km 5.300, Boadilla del Monte, Madrid 28668, Spain, [b]Institut Laue–Langevin, 6 Rue Jules Horowitz, Grenoble, Isere/Rhone-Alpes 38042, France, [c]Química Inorgánica, Facultad de Ciencias Químicas, Universidad Complutense de Madrid, Avenida Complutense s/n, Madrid 28040, Spain, [d]SpLine Spanish CRG Beamline, ESRF, 6 Rue J. Horowitz, Grenoble, Isere/Rhone-Alpes 38042, France, and [e]Instituto de Ciencia de Materiales de Madrid-ICMM/CSIC, Sor Juana Inés de la Cruz 3, Madrid 28049, Spain. *Correspondence e-mail: a.gomez126@usp.ceu.es, uamador@ceu.es

The evolution of the room-temperature structure of the oxide series $La_{2-x}Sr_xCoTiO_6$ ($0.6 \leq x \leq 1.0$) was studied as a function of the Sr content using different diffraction techniques and applying the symmetry-adapted modes formalism (*AMPLIMODES*). The title compounds adopt perovskite-like structures of rhombohedral symmetry with an octahedral tilting scheme ($a^-a^-a^-$) with either space group $R\bar{3}c$ or $R32$. The latter symmetry is observed in those cases (for $x \simeq 0.6$) where additional rock-salt-like ordering of La and Sr is produced in the perovskite *A* sites. Two composition-driven phase transitions are observed in the whole series $La_{2-x}Sr_xCoTiO_6$ ($0.0 \leq x \leq 1.0$). Using the concept of internal pressure, the effect of doping with Sr on the structure can be properly discussed. Both phase transitions seem to be of first order since they can be associated with discontinuities either in the entropy or in the structure. The first transition ($P2_1/n \rightarrow Pnma$) occurs as the *B* cations become totally disordered. Along the whole compositional range the modes responsible for the out-of-phase tilting of BO_6 octahedra remain active, but those associated with the in-phase octahedral tilting vanish for $x \geq 0.6$, this being associated with the second transition ($Pnma \rightarrow R\bar{3}c$). Finally, for $x = 1.0$ the three pseudo-cubic cell parameters become very similar, pointing to a transition to a cubic structure which could be obtained by applying pressure or raising the temperature.

1. Introduction

It is well known that perovskite-like oxides (with formula ABO_3, or the more complex double perovskites with composition $AA'BB'O_6$) are highly versatile in composition, structure and properties (Mitchell, 2002; Ishihara, 2009; Orlovskaya & Browning, 2004), making them potentially useful for many applications. In particular, some of them may be used as cathodes for solid oxide fuel cells (SOFCs), inasmuch as they present high electronic and ionic conductivity due to the simultaneous presence of cations with mixed oxidation states and of anionic (oxygen) vacancies (Adler, 2004; Fergus, 2006; Ishihara *et al.*, 2004; Mitchell, 2002; Trofimenko, 1999), as well as an adequate catalytic activity (Liu *et al.*, 2007; Sun *et al.*, 2009). In this context, a convenient doping strategy of the parent materials, on either the *A* or the *B* sites, allows modification of the oxidation states of *B* cations as well as the creation of mobile oxygen vacancies, inducing mixed conduction.

Many perovskites undergo phase transitions driven by different thermodynamic parameters, mainly temperature and pressure (Mountstevens *et al.*, 2003; Zhao *et al.*, 2009; Khom-

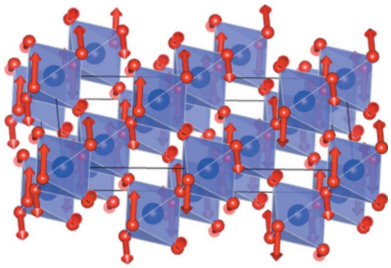

chenko *et al.*, 2013). These phase transitions can be classified into two main categories: (*a*) those mostly due to structural distortions produced by correlated atomic displacements which lower the symmetry of the parent structure (displacive transitions) and (*b*) those with a dominant order–disorder component with symmetry-breaking changes of the occupation probabilities of some atomic sites (order–disorder transitions).

In the framework of our research on materials for SOFC cathodes we have explored several perovskite-like oxides (Maupoey *et al.*, 2012; Pérez-Flores *et al.*, 2012, 2013; Yuste *et al.*, 2011; Maupoey *et al.*, 2014). In particular we prepared the series $La_{2-x}Sr_xCoTiO_6$ ($0 \leq x \leq 1.0$) in which different structures are observed depending on the Sr content (Yuste *et al.*, 2011).

In a previous paper (Gómez-Pérez *et al.*, 2014) the room-temperature structure of the series members $La_{2-x}Sr_xCoTiO_6$ ($0 \leq x \leq 0.5$) as a function of the Sr content was determined. The combined use of synchrotron radiation high-resolution powder diffraction, neutron powder diffraction, and high-resolution electron microscopy and electron diffraction allowed the determination of the structures. A symmetry-adapted formalism which reveals the physical origin of the distortions responsible for the phase transitions was used to discuss the transitions between the different structures in these compounds. The evolution of the amplitudes of the primary modes R_4^+ (associated with the out-of-phase tilting of BO_6 octahedra) and M_3^+ (associated with the in-phase octahedral tilting) with the Sr content suggested a phase 'transition' for $x > 0.5$. The symmetry of this new phase will be determined by the remaining primary active mode (with nonzero amplitude) R_4^+. Therefore, the expected symmetry of the new structure was predicted to be that of the isotropy group of the basis mode of the irreducible representation (Irrep) R_4^+, *i.e.* space group (SG) *Imma* with tilting scheme ($a^-a^-c^0$). Although this symmetry is not common in perovskites, some cases such as $BaCe_xZr_{1-x}O_3$ have been reported in which a clear transition sequence $Pnma \rightarrow Imma \rightarrow R\bar{3}c$ has been determined for increasing Zr doping (Pagnier *et al.*, 2000). The stability field (in terms of composition and temperature) of the *Imma* structure seems to be pretty narrow. Since the orientation of the order parameter associated with the mode easily changes through a first-order phase transition, two possible directions can be considered:

(1) ($a00$), yielding an SG $I4/mcm$ with tilting scheme ($a^0a^0c^-$) and

(2) (aaa) to give a tilting scheme ($a^-a^-a^-$) and SG $R\bar{3}c$.

Examples for these two possibilities are found in the literature in temperature-driven phase transitions. Thus, $SrZrO_3$ (Howard & Stokes, 1998; Kennedy *et al.*, 1999) and $Sr_{1-x}Ba_xSnO_3$ (Mountstevens *et al.*, 2003) are examples of the tetragonal case, whereas $BaCeO_3$ (Knight, 1994) is an example of the rhombohedral symmetry.

In the present paper we report a study of the upper compositional range ($0.6 \leq x \leq 1.0$) of the $La_{2-x}Sr_xCoTiO_6$ series. The phase transitions found throughout the whole family and the effect of temperature and pressure are discussed. A transition to a cubic structure is also predicted. In this connection, the thermal evolution of the structure of some selected members of the $La_{2-x}Sr_xCoTiO_6$ series ($0 \leq x \leq 1.0$) will be published in due course.

2. Experimental

2.1. Samples

Samples of compositions $La_{2-x}Sr_xCoTiO_6$ ($0.6 \leq x \leq 1.0$) were prepared by a modified Pechini method from high-purity $Co(CH_3COO)_2{\cdot}4H_2O$ (Aldrich, 99.99%), La_2O_3 (Aldrich, 99.9%), $SrCO_3$ (Aldrich 99.9%) and TiO_2 (anatase, Aldrich, purity 99.9%) as previously reported (Yuste *et al.*, 2011).

2.2. Experimental techniques

The purity of the samples was determined by powder X-ray diffraction (XRD) on a Bruker D8 high-resolution diffractometer, using monochromatic Cu $K\alpha_1$ (λ = 1.5406 Å) radiation obtained with a germanium primary monochromator, and equipped with a solid-state rapid LynxEye detector.

Synchrotron radiation high-resolution powder X-ray diffraction (SXRD) patterns were collected on SpLine, the Spanish CRG beamline BM25A, at the European Synchrotron Radiation Facility (ESRF), Grenoble (France). A detailed description of the apparatus is given by Rubio-Zuazo *et al.* (2013) and Castro (1998). The samples were finely ground and loaded into a 0.4 mm-diameter capillary mounted in a spinning goniometer. Room-temperature data were collected in a continuous 2θ scan mode from 7 to 48° using an incident wavelength of 0.62100 (6) Å [calibrated with NIST SRM 640c silicon powder; a = 5.431195 (9) Å]. The counts from the different channels were rebinned to produce an equivalent normalized step scan of 0.01° step intervals, with a count time of 1 s per step. Neutron powder diffraction (NPD) experiments at room temperature were performed on the high-resolution diffractometer D2B at the Institut Laue–Langevin. A monochromatic beam of wavelength 1.5940 Å was selected with a Ge monochromator from the primary beam, the divergence of which was defined by an additional 10′ collimator to increase the instrumental resolution. The structural refinements were carried out by the Rietveld method by the joint fitting of SXRD and NPD data, using the *AMPLIMODES* formalism (Perez-Mato *et al.*, 2010; Orobengoa *et al.*, 2009) implemented in the *FullProf* program (Rodríguez-Carvajal, 1993). The neutron scattering amplitudes used in the refinement were 0.824, 0.702, 0.249, −0.344 and 0.581 (10^{-12} cm) for La, Sr, Co, Ti and O, respectively.

Selected area electron diffraction, convergent beam electron diffraction (CBED) and high-resolution electron microscopy (HREM) were performed using a JEOL 3000FEG electron microscope, fitted with a double tilting goniometer stage (±25°, ±25°). Simulated HREM images were calculated by the multislice method using the *MacTempas* software package (R. Kilaas, Total Resolution, Berkeley, CA, USA).

3. Results

3.1. Samples

Conventional X-ray diffraction data (not shown) revealed that most batches of the different compositions are single phase and well crystallized materials. However, in some cases for the highest Sr containing samples small amounts (*ca* 3% weight) of CoO and/or $SrTiO_3$ are present.

3.2. Unit-cell and symmetry determination

As done in previous papers (García-Martín *et al.*, 2004; Gómez-Pérez *et al.*, 2014), we tackled the structure determination of the title materials using complementary techniques. In perovskite oxides, correlated displacements of light oxygen atoms are responsible for important structural features. Order–disorder phenomena involving elements with similar atomic numbers (Co/Ti), and consequently similar numbers of electrons, can also exist. X-ray diffraction (using either laboratory or synchrotron sources) is not suitable to deal with these issues. These limitations can, however, be overcome using neutron diffraction techniques. The complementary use of SXRD and NPD data for a joint data fitting and structure refinement provides a powerful tool to fully determine the structural features of perovskite-like oxides. The high peak-to-peak resolution given by SXRD allows the determination of the unit cell of the material. Owing to the short correlation length, electron diffraction and microscopy provide crucial information to develop the correct structural model or to confirm the models proposed on the basis of other techniques. In particular HREM gives projections of the real space (the atoms in the structure) that are often very useful to test the validity of a given model (see *e.g.* García-Martín *et al.*, 2004).

We used the program *AMPLIMODES* (Orobengoa *et al.*, 2009; Perez-Mato *et al.*, 2010) to analyse our diffraction data, as already done for the low Sr containing oxides of the series $La_{2-x}Sr_xCoTiO_6$ ($0 \leq x \leq 0.5$) (Gómez-Pérez *et al.*, 2014). The mode-decomposition formalism applied considers any structure as resulting from the distortion of a virtual aristotype structure through a series of collective displacements of atoms. The needed starting information on the actual ('distorted') structure is the SG, the unit cell and the number of formula units per unit cell (Z). A model for the virtual aristotype structure is also needed.

In the case of $La_{2-x}Sr_xCoTiO_6$ ($0.6 \leq x \leq 1.0$) one only needs one aristotype structure since the whole series presents the same symmetry and all members can be fully explained as derived from the $Pm\overline{3}m$ cubic structure.

As a first step the SG of the materials has to be defined unambiguously and a reliable unit cell has to be determined by using the SXRD/XRD data in a LeBail fitting process (Le Bail *et al.*, 1988). The smallest unit cell that accounts for all the reflections is $a \simeq b = 2^{1/2}a_p$, $c = 2(3^{1/2})a_p$, $\alpha = \beta = 90^\circ$ and $\gamma = 120^\circ$, (a_p being the cell parameter of the cubic perovskite aristotype), which is a very common cell in perovskite oxides with rhombohedral symmetry (Mitchell, 2002).

The structure evolution of $La_{2-x}Sr_xCoTiO_6$ ($0 \leq x \leq 0.5$) compounds revealed that in this compositional range the octahedral tilting scheme is $(a^-a^-c^+)$: the modes responsible for the out-of-phase tilting of the BO_6 octahedra remain active but those associated with the in-phase tilting decrease and become negligible for $x = 0.5$, anticipating for $x \geq 0.6$ a transition to a new structure with tilting scheme either $(a^0a^0c^-)$ (SG *I*4/*mcm*) or $(a^-a^-a^0)$ (SG *Imma*) or $(a^-a^-a^-)$ (SG $R\overline{3}c$) (Gómez-Pérez *et al.*, 2014).

Table 1
Structural parameters of the perovskite aristotypes given in both the high-symmetry (SG $Pm\overline{3}m$) and the low-symmetry settings (SG $R\overline{3}c$) and the corresponding transformation matrix for the high- to the low-symmetry phases.

Aristotype structure
Space group: $Pm\overline{3}m$
Cell parameter: $a = 3.9129$ Å, $Z = 1$

Atom	Wyckoff position	x	y	z
La/Sr	1*b*	1/2	1/2	1/2
Co/Ti	1*a*	0	0	0
O	3*d*	1/2	0	0

↓

SG $R\overline{3}c$

$$\left(\begin{array}{ccc|c} 0 & 1 & 2 & 0 \\ -1 & 0 & 2 & 0 \\ 1 & -1 & 2 & 0 \end{array}\right)$$

↓

Low-symmetry structure
Cell parameters: $a = 5.5337$, $b = 5.5337$, $c = 13.5547$ Å, $Z = 6$

Atom	Wyckoff position	x	y	z
La/Sr	6*a*	0	0	1/4
Co/Ti	6*b*	0	0	0
O1	18*e*	1/6	1/3	1/12

Since for $x \geq 0.6$ the cell is rhombohedral, structural models such as $(a^0a^0c^-)$ (SG *I*4/*mcm*) or $(a^-a^-a^0)$ (SG *Imma*) can be discarded. Thus, using the results from group theory analysis our experimental data allow the unambiguous assignment of the SG $R\overline{3}c$ as the materials' actual symmetry, with a tilt scheme $(a^-a^-a^-)$ (Glazer, 1972), provided no cation ordering exists and the distortion from the aristotype is only due to BO_6 octahedral tilting (Woodward, 1997*a*,*b*; Howard & Stokes, 1998). As the unit cell and SG are unambiguously determined, the transformation matrix from the aristotype ($Pm\overline{3}m$) to the actual symmetry can be calculated. Table 1 presents the unit cell of the high- and low-symmetry structures, the transformation matrix linking them, and the structural parameters of the aristotype given in both the high- and the low-symmetry settings. All this information is used in the mode-decomposition process. In Table 2 the actual cell parameters and SG determined for our materials are presented.

Using the information on the symmetry of the aristotype and the distorted structures and the transformation matrix linking them, *AMPLIMODES* calculates the decomposition into basis modes.

The starting amplitudes of the modes are obtained *ab initio* from the integrated intensities of the NPD patterns extracted by the LeBail method (Le Bail *et al.*, 1988), which are used in a 'simulated-annealing' iteration. Good starting amplitudes for

Table 2
Unit-cell parameters and symmetry determined for the $La_{2-x}Sr_xCoTiO_6$ ($0.6 \leq x \leq 1.0$) perovskites.

	X-ray source	SG	a (Å)	b (Å)	c (Å)
$La_{1.40}Sr_{0.60}CoTiO_6$	Synchrotron	$R\bar{3}c$	5.5123 (2)	5.5123 (2)	13.3707 (4)
$La_{1.30}Sr_{0.70}CoTiO_6$	Conventional diffractometer	$R\bar{3}c$	5.4975 (3)	5.4975 (3)	13.3615 (8)
$La_{1.20}Sr_{0.80}CoTiO_6$	Synchrotron	$R\bar{3}c$	5.4833 (2)	5.4833 (2)	13.3434 (5)
$La_{1.10}Sr_{0.90}CoTiO_6$	Conventional diffractometer	$R\bar{3}c$	5.4813 (3)	5.4813 (3)	13.3580 (6)
$La_{1.00}Sr_{1.00}CoTiO_6$	Synchrotron	$R\bar{3}c$	5.4716 (2)	5.4716 (2)	13.3583 (4)

the modes ensure a robust refinement process, resulting in good structural models.

Finally, as indicated in the *Experimental* section the structure refinements were performed by simultaneous fitting of the SXRD and NPD patterns; the refined structural parameters being the amplitudes of each individual mode.

3.3. Crystal structure

The mode decomposition of the symmetry breaking $Pm\bar{3}m \rightarrow R\bar{3}c$ and the refined amplitudes for the title compounds are given in Tables 3 and 4, respectively.

The symmetry breaking proceeds through one single mode whose symmetry is given by the irreducible representation $R_4^+(1)$ (being of primary nature since the isotropy group of the Irrep is sufficient to explain the observed symmetry). The number of modes transforming according to the irreducible representation is given in parentheses. Table 4 presents the direction of the order parameter and the propagation vector for the basis mode acting in the $Pm\bar{3}m$ to $R\bar{3}c$ transition, the amplitudes of this mode (in Å), and its associated isotropy group (*i.e.* the symmetry resulting by the sole action of the given mode).

Table S1 collects the structural models (in terms of atomic positions) refined by *AMPLIMODES*, while Table S2 shows selected structural information. Graphical results of the data fitting of SXRD and NPD data are depicted in Fig. S1.

The effect of the unique Irrep mode is depicted in Fig. 1; it consists of rotations of the oxygen atoms around the c axis, alternating the sense of the rotation from one layer to the next. Thus, it is responsible for the out-of-phase tilt present in these perovskites. This is the only long-range structural effect responsible for the phase evolution from the high-symmetry structure to the actual-symmetry ones. However, in some cases local effects can be seen by transmission electron microscopy (TEM) and HREM. Although the coherence lengths of NPD and XRD limit the information on local effects given by these techniques, in those cases for which TEM and HREM revealed significant additional structural features, they have been included in the final models given in Tables S1 and S2.

It is readily seen from the amplitudes of the modes that as the Sr content increases the structure becomes less distorted, suggesting that the internal stress of the structure is relieved as a consequence of a better matching of $A-O$ and $B-O$ bonds. Eventually, a transition to the cubic $Pm\bar{3}m$ aristotype should occur if more La could be replaced by Sr. In this context, we have tried to prepare material with $x = 1.10$ and 1.20 without success; in all cases segregation of $LaCoO_3$ and $SrTiO_3$ is produced. Sugahara & Ohtaki (2011) reported the existence of compounds $Sr_{2-x}La_xCoTiO_6$ in the whole compositional range ($0 \leq x \leq 2$) though no detailed structure characterization was given.

An electron microscopy study of $La_{2-x}Sr_xCoTiO_6$ oxides was performed to confirm, at the local level, the average

Table 3
Symmetry-mode decomposition of the structure distortion from the aristotype cubic perovskite $Pm\bar{3}m$ to the rhombohedral phase ($R\bar{3}c$) and the atoms over which each mode acts.

Atom	Wyckoff position	Mode
O1	18*e*	$R_4^+(1)$

Table 4
Summary of the mode decomposition, after simultaneous fitting of SXRD and NPD data at RT, for the $Pm\bar{3}m$ to $R\bar{3}c$ evolution.

R_4^+ is the primary Irrep mode. Samples are indicated by their Sr content, x in $La_{2-x}Sr_xCoTiO_6$

K vector	Irrep	Direction	Isotropy subgroup	Dimension	Amplitude (Å)	
$(\frac{1}{2}, \frac{1}{2}, \frac{1}{2})$	R_4^+	(*aaa*)	$R\bar{3}c$	1	$x = 0.60$ 0.5953 (16)	$x = 0.70$ 0.5444 (19)
					$x = 0.80$ 0.4895 (14)	$x = 0.90$ 0.4346 (16)
					$x = 1.00$ 0.3991 (21)	

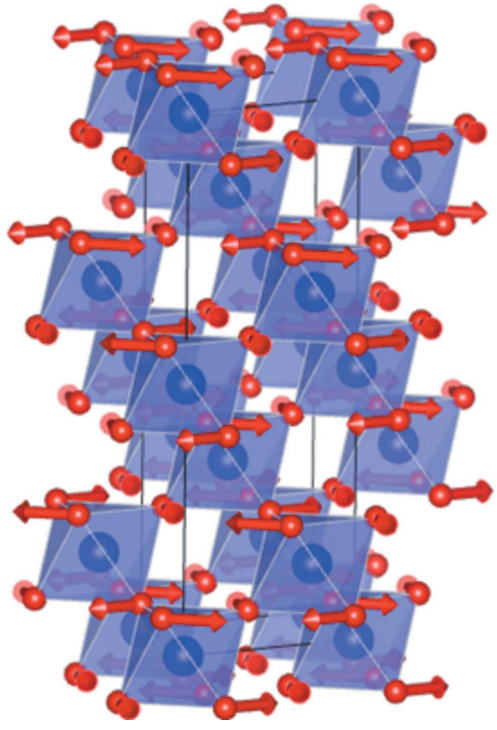

Figure 1
Pictorial representation of the symmetry-adapted displacement pattern of atoms, Irrep mode R_4^+ [out of-phase tilting of BO_6 octahedra (in blue)], which results in the $R\bar{3}c$ structure from the ideal cubic ($Pm\bar{3}m$) structure.

structural model obtained by XRD and NPD. Some unexpected and interesting results are obtained for the $x = 0.6$ ($La_{1.4}Sr_{0.6}CoTiO_6$) member of the series. Figs. 2 and 3 show typical images taken on crystallites of this sample along the zone axes $[1\bar{1}0]_p$ and $[1\bar{2}1]_p$, respectively.

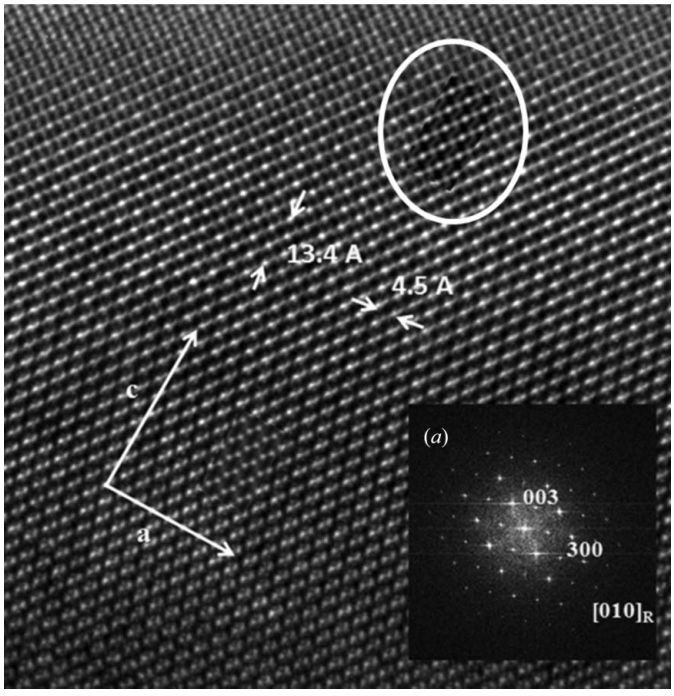

Figure 2
HREM image of $La_{1.4}Sr_{0.6}CoTiO_6$ along $[110]_p$. (*a*) Optical FFT of the image. A simulated image corresponding to the marked area is shown ($\Delta t = 5$ nm and $\Delta f = -30$ nm).

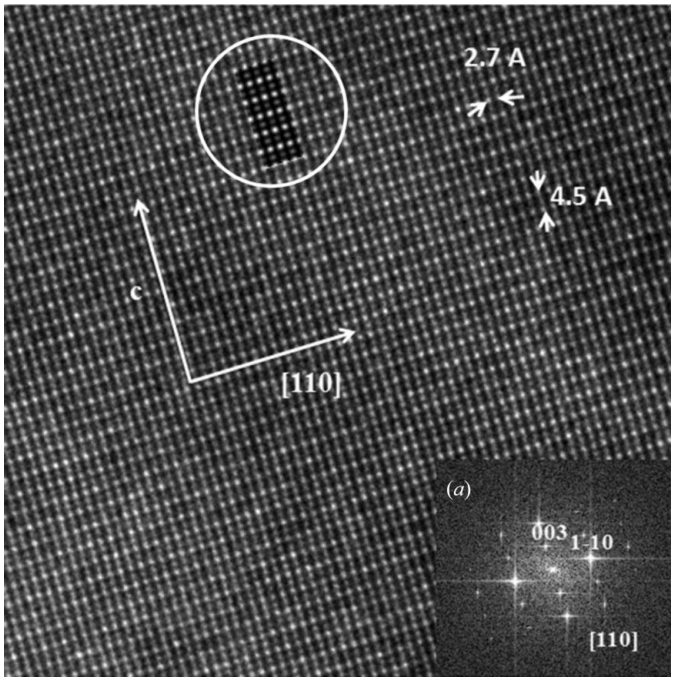

Figure 3
HREM image of $La_{1.4}Sr_{0.6}CoTiO_6$ along $[1\bar{2}1]_p$. (*a*) Optical FFT of the image. A simulated image corresponding to the marked area is shown ($\Delta t = 5$ nm and $\Delta f = -30$ nm).

At first sight one can observe a much more complex microstructure than expected from powder diffraction data. Although the spots observed in the fast Fourier transform (FFT) can be indexed on the basis of a double cubic perovskite unit cell, the corresponding high-resolution image, shown in Fig. 2, suggests a different situation. A careful analysis of the HREM image reveals an ordering of atoms in the perovskite *A* sites, with layers of composition LaO and (La/Sr)O alternating along the *c* axis. The FFT shown in Fig. 2(*a*) suggests a rhombohedral symmetry, with *d* spacings of 4.5 and 13.4 Å that corresponds to the d_{100} and d_{001} values.

The HREM image along $[1\bar{1}0]_R$ (Fig. 3) confirms this model. After a careful analysis, this micrograph reveals planes with *d* spacings of 2.7 and 4.5 Å, corresponding to d_{110} and d_{001}.The contrast variation confirms the existence of two different layers alternating along the c_R axis: layers of bright dots and less-bright dots [corresponding to LaO layers alternating with (La/Sr)O ones]. The optical Fourier transform corresponding to this image is depicted in Fig. 3(*a*).

All reflections in Figs. 2(*a*) and 3(*a*) can be indexed on the basis of a rhombohedral unit cell with parameters $a = 5.5$ Å and $c = 13.4$ Å. The reflection conditions are compatible with the space groups *R*3 (No. 146), $R\bar{3}$ (No. 148), *R*32 (No. 155), *R*3*m* (No. 160) and $R\bar{3}m$ (No. 166). Since the symmetries of the projection along [001] of these SGs are different a CBED study was performed along this direction to determine the actual symmetry of this compound. As shown in Fig. 4 the symmetry of this material projected along the *c* axis is *p*3*m*1, suggesting the *R*32 rhombohedral symmetry (Hahn, 2005).

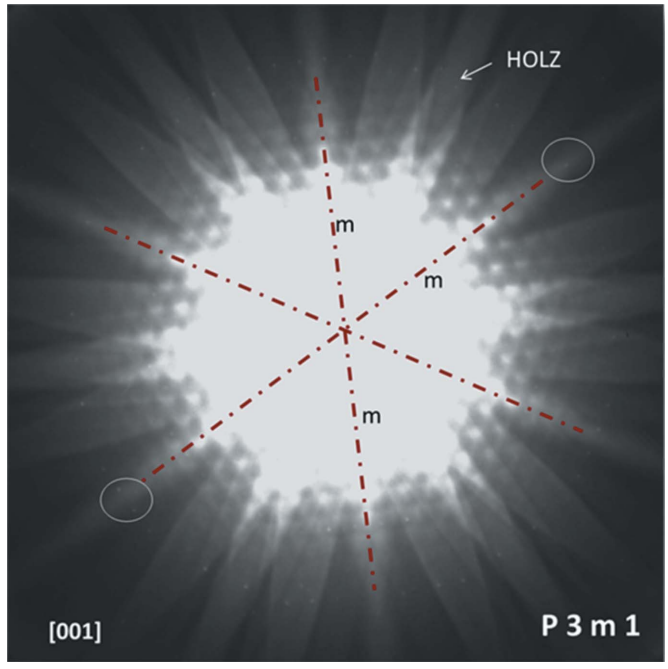

Figure 4
Convergent beam electron diffraction pattern along [001] for $La_{1.4}Sr_{0.6}CoTiO_6$, showing a *p*3*m*1 symmetry.

The SG $R\bar{3}c$ used to develop the structural model from XRD and NPD precludes any kind of cationic ordering either on the *A* or on the *B* sites. Therefore, a new model with *R*32 symmetry must be proposed to account for the observed order of the *A* ions.

The *A*-site layered arrangements commonly present in perovskites, consisting of sheets of *A* ions with different compositions alternating along one of the a_p axes, cannot be described in a rhombohedral lattice (Howard & Zhang, 2004). The layered *A*-site ordering found in $La_{1.4}Sr_{0.6}CoTiO_6$ is, in fact, due to a rock-salt arrangement of *A* ions (different ions alternate along the three a_p axes). This ordering results in layers of different compositions alternating along the $[111]_p$ direction, which is the *c* axis of the rhombohedral cell (using the hexagonal setting, in fact $c_R = 2\ d_{(111)p}$).

A new model was then developed to treat the diffraction data and for image calculation. Although the simulated images fit nicely to the experimental ones (Figs. 2 and 3), the fits of the powder diffraction patterns yield somewhat unsatisfactory results. In particular there are very weak reflections that should appear in our patterns (especially in the X-ray ones) which are totally absent (Fig. S1). This points to a local or short-range nature of the A-ion ordering and explains why the reflections associated with such features are absent in the XRD and NPD patterns (Dachraoui *et al.*, 2011). For completeness the refined parameters of this model for $La_{1.4}Sr_{0.6}CoTiO_6$ are given in Table S3; similar information for the other compositions is not included since the evidence for A-ion ordering is not clear (see below).

The HREM micrograph along the $[010]_R$ zone axis of $LaSrCoTiO_6$ depicted in Fig. 5 is much more complex than that of $La_{1.4}Sr_{0.6}CoTiO_6$ (Fig. 2). A careful analysis of the HREM image reveals some areas with additional ordering of the perovskite A ions. The FFT shown in Fig. 5(*a*) suggests a rhombohedral symmetry, with *d* spacings of 4.5 and 13.4 Å, corresponding to the d_{100} and d_{001} planes, respectively. A small area with a simple perovskite structure is also observed (zone A).

The HREM image along $[1\bar{1}0]_R$ (Fig. 6) shows planes with *d* spacings of 2.7 and 2.2 Å, corresponding to d_{110} and d_{006}.The contrast variation does not reveal the existence of large areas with layered A ions ordered along the c_R axis, in contrast to what is observed for the previous composition, $La_{1.4}Sr_{0.6}CoTiO_6$. The optical Fourier transform of this image is shown in Fig. 6(*a*). All reflections in Figs. 5(*a*) and 6(*a*) can be indexed on the basis of a rhombohedral unit cell with parameters a = 5.5 Å and c = 13.4 Å. Although the images show less ordering than for the $x = 0.6$ member of the series, again the reflection conditions are compatible with the *R*32 space group. Thus, simulated images using an ordered model fit nicely to the experimental ones (see Figs. 5 and 6).

It seems that the introduction of more Sr atoms along the $La_{2-x}Sr_xCoTiO_6$ series tends to equilibrate the La/Sr ratio among the (LaSr)O layers, reducing as well the local *A*-site ordering.

4. Structure evolution along the series $La_{2-x}Sr_xCoTiO_6$ ($0 \leq x \leq 1.0$)

We recall that phase transitions can be induced in a system by modifying any of its thermodynamic parameters. Pure structural transitions are usually pressure and/or temperature

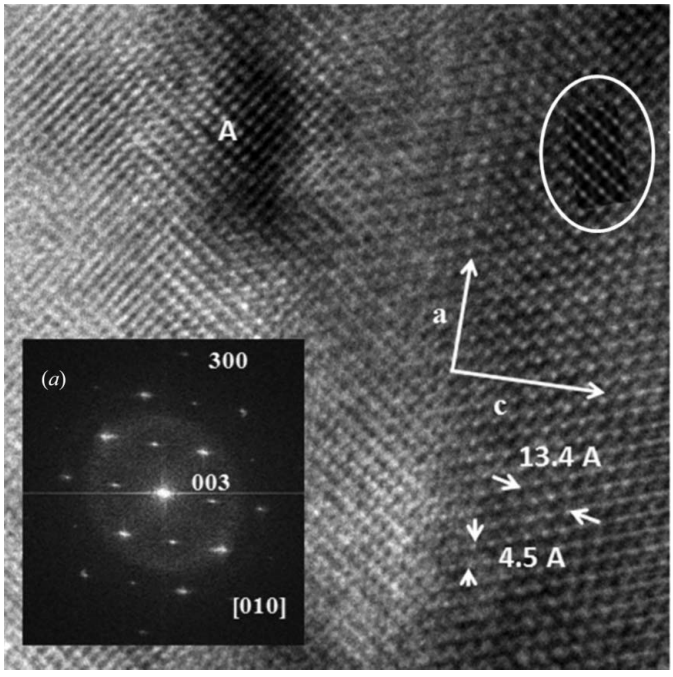

Figure 5
HREM image of $La_{1.0}Sr_{1.0}CoTiO_6$ along $[110]_p$ ($[010]_R$). (*a*) Optical FFT of the image. A simulated image is shown (Δt = 5 nm and Δf = −30 nm).

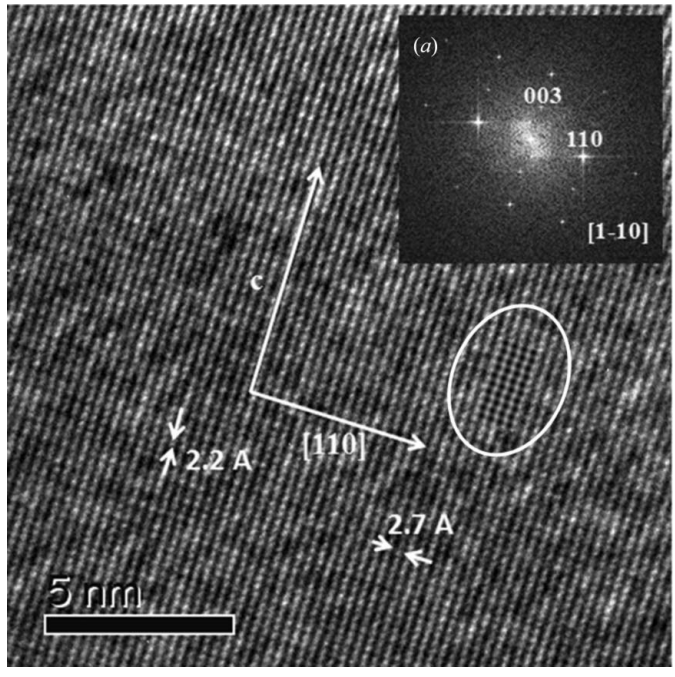

Figure 6
HREM image of $La_{1.0}Sr_{1.0}CoTiO_6$ along $[1\bar{2}1]_p$ ($[1\bar{1}0]_R$). (*a*) Optical FFT of the image. A simulated image is shown (Δt = 5 nm and Δf = −30 nm).

driven; however, in this study, the chemical composition is the driving force. At this point the concept of 'chemical pressure' has to be introduced, describing an equivalent pressure (which can be positive–compressive or negative–expansive) induced in a structure by the chemical substitution of one element for another of different size (smaller or larger, respectively) (Djurado *et al.*, 2003). For our system Fig. 7 shows the evolution of the normalized lattice parameters (including cell volume) as a function of increasing Sr content. It can be readily seen that a cell contraction occurs as $^{XII}La^{3+}$ (r = 1.36 Å) is replaced by a larger cation $^{XII}Sr^{2+}$ (r = 1.44 Å) (Shannon, 1976). This apparently contradictory result can be easily explained. In a previous paper (Yuste *et al.*, 2011) it has been demonstrated that the main charge compensating mechanism for the aliovalent La^{3+}/Sr^{2+} substitution is the oxidation of Co^{2+} to Co^{3+}. Although it is difficult to assign a value for the ionic radius of Co^{3+} ions owing to the multiple spin states that they can adopt in oxides (Raveau & Seikh, 2012; Yuste *et al.*, 2011), it is evident that an increase of the oxidation state results in a decrease of the cation size. This effect seems to be dominant over the increase of the size of the *A*-site cation upon substitution, and a lattice contraction is observed; consequently, compressive pressure is induced.

In a previous paper (Gómez-Pérez *et al.*, 2014) we reported the structural evolution found for $La_{2-x}Sr_xCoTiO_6$ in the compositional range ($0 \leq x \leq 0.5$); in the present work the compositional range up to $x = 1.0$ has been studied in order to complete the picture. For low Sr contents (up to $x = 0.2$) the structure is monoclinic (SG $P2_1/n$), whereas in the range ($0.3 \leq x \leq 0.5$) an orthorhombic (SG *Pnma*) structure is adopted (Fig. 8). The structural evolution was also studied using the mode-decomposition formalism. The evolution of the primary modes, those which are mainly but not solely responsible for the distortion of the actual structure from the high-symmetry aristotype, allows explanation or even prediction of the structural transitions. As shown in Fig. 8 the modes X_3^+/M_3^+ and GM_4^+/R_4^+ (the symbols of the corresponding Irreps are different for $P2_1/n$ and *Pnma* but the physical effect is the same) associated with in-phase and out-of-phase BO_6-octahdra tilting, respectively, continuously decrease along the compositional range ($0.0 \leq x \leq 0.5$). This is a signature of the release of structure distortion and the tendency to adopt a more symmetric structure.

Interestingly, the mode X_3^+/M_3^+ – and consequently the in-phase tilting – vanishes for $x > 0.5$, whereas the out-of-phase tilt does not. Thus, the evolution of the amplitudes of the modes suggests a phase transition for this composition.

However, the transition $P2_1/n \rightarrow Pnma$ cannot be predicted, or explained, by the evolution of the modes. Indeed, in the compositional border for this transition, $x > 0.2$, both X_3^+/M_3^+ and GM_4^+/R_4^+ modes describing the same ($a^-a^-c^+$) tilting scheme for the monoclinic and orthorhombic structures vary smoothly. The explanation for this is the fact that the mode-decomposition formalism as implemented in *AMPLIMODES* deals with displacive phase transitions and can therefore not predict phase transitions of order–disorder nature. In Fig. 8 the degree of *B* order is plotted (Gómez-Pérez *et al.*, 2014); from its evolution with the Sr content it is evident that the $P2_1/n \rightarrow Pnma$ transition occurs when this parameter becomes zero. On the other hand, the $Pnma \rightarrow R\bar{3}c$ transition is clearly anticipated by the disappearance of the M_3^+ mode, and correspondingly of the in-phase tilting, for $x >$ 0.5. Among the different structures that the fading of this mode can originate [($a^0a^0c^-$) (SG *I*4/*mcm*), ($a^-a^-a^0$) (SG *Imma*) or ($a^-a^-a^-$) (SG $R\bar{3}c$)], we unambiguously determined the structure of the high Sr content materials to be rhombohedral, resulting as a consequence of the reorientation of the order parameter of the R_4^+ mode in the transition [from (0*aa*) to (*aaa*) direction].

Discussing the order of these transitions, one knows that first-order phase transitions are characterized by a discontinuity in the first derivative of the Gibbs energy (Landau & Lifshitz, 1959; Tolédano & Toléadano, 1987) (*i.e.* the cell volume and the entropy, usually expressed as a latent heat).

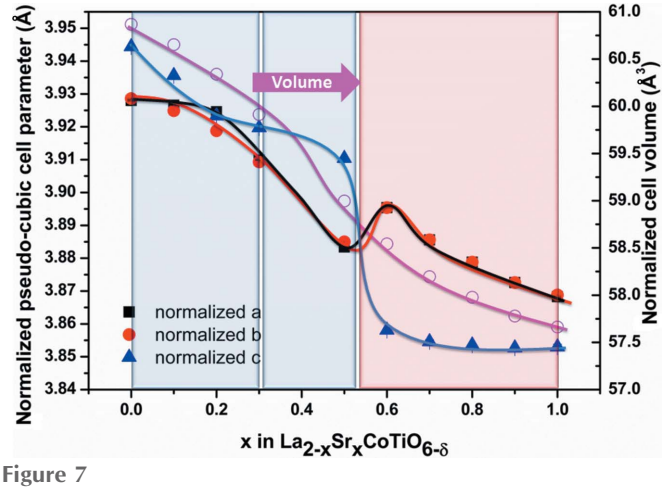

Figure 7
Evolution of the normalized pseudo-cubic cell parameters and reduced volume along the $La_{2-x}Sr_xCoTiO_6$ ($0 \leq x \leq 1.0$) series. Lines are guides for the eye.

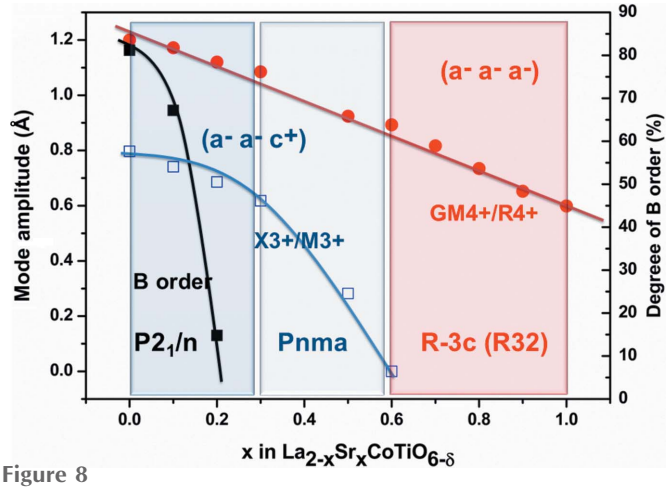

Figure 8
Evolution of the mode amplitudes with the Sr content for $La_{2-x}Sr_x$-$CoTiO_6$ ($0.0 \leq x \leq 1.0$); the degree of *B*-ion order for $x < 0.3$ is also plotted. Lines are guides for the eye.

The evolution of the normalized volume with x, shown in Fig. 7, does not show any abrupt changes. However, looking at the changes of the individual lattice parameter as a function of the Sr content a clear discontinuity is observed for all three cell parameters at $0.5 \leq x \leq 0.6$ corresponding to the $Pnma \rightarrow R\overline{3}c$ transition, suggesting that this is of first-order nature. Conversely, in the $P2_1/n \rightarrow Pnma$ transition ($0.2 \leq x \leq 0.3$) no evident discontinuity of the structure is observed. Nevertheless, it is clear that in the case of order–disorder transitions an abrupt variation of the configurational entropy is produced (in the present case associated with B-site ordering, see Fig. 8). In the case of the $Pnma \rightarrow R\overline{3}c$ transition the change of the direction of the order parameter (mode R_4^+ associated with the out-of-phase tilt) is also related to a change in entropy, mainly due to variations in the vibrational energy (Dove, 1997). Thus, the two phase transitions observed in the $La_{2-x}Sr_xCoTiO_{6-\delta}$ series as a function of the Sr content can be assumed to be first order.

The above results are in very good agreement with what has been predicted by Magyari-Köpe *et al.* (2002). They claim that applying hydrostatic pressure tends to stabilize less distorted (high-symmetry) phases; note that a similar tendency is observed by increasing the temperature. Although the data here presented are taken at ambient temperature and pressure, the replacement of La^{3+} by Sr^{2+} is equivalent to the application of external pressure. As stated above, in the series $La_{2-x}Sr_xCoTiO_6$ the aliovalent substitution results in a compressive pressure which tends to stabilize high-symmetry phases. In this context there are many examples in the literature of perovskite-like materials, such as $LaGaO_3$, $LaCrO_3$ and $LaFeO_3$, which present a pressure-driven transition $Pnma \rightarrow R\overline{3}c$ similar to the one discussed here (Shibasaki *et al.*, 2005; Kennedy *et al.*, 2001; Zhou *et al.*, 2011). However, some other perovskites do not evolve in the same way (Alexei & Wei, 2014), most probably as these materials present a strong covalent character (Magyari-Köpe *et al.*, 2002). A nice example of the equivalent effect of pressure (internal) and temperature on the structure evolution is described in the perovskite series $BaCe_xZr_{1-x}O_3$ whose structures become more symmetrical for increasing Zr doping (Pagnier *et al.*, 2000).

Finally, we stress that for $x = 1.0$ the convergence of the three pseudo-cubic parameters (Fig. 7) anticipates a transition to a cubic phase, which could be obtained for $x > 1.0$ (unfortunately we did not succeed in preparing pure materials with such high levels of Sr content), applying pressure or at high temperature. The thermal evolution of the structure of selected materials of the $La_{2-x}Sr_xCoTiO_{6-\delta}$ ($0 \leq x \leq 1.0$) series will be published in due course.

5. Concluding remarks

The evolution of the room-temperature structure of the oxides $La_{2-x}Sr_xCoTiO_6$ studied as a function of increasing Sr content shows that a cell contraction occurs as La^{3+} is replaced by the larger cation Sr^{2+}. This apparently contradictory result can be explained by the oxidation of Co^{2+} to Co^{3+}, with the concomitant size reduction, as the main charge compensating mechanism for the aliovalent La^{3+}/Sr^{2+} substitution. This effect dominates over the increase of the size of the A cation, and consequently compressive internal pressure is induced in the material. Two composition-driven phase transitions are observed in the whole series $La_{2-x}Sr_xCoTiO_6$ ($0.0 \leq x \leq 1.0$). These phase transitions are discussed using the concept of internal pressure and a symmetry-adapted formalism together with the concept of modes (which reveal the physical origin of the distortions responsible for the actual structures).

The first transition ($P2_1/n \rightarrow Pnma$) occurs as the B cations become completely disordered for $x > 0.20$, but the two modes X_3^+/M_3^+ and GM_4^+/R_4^+ describing the same ($a^-a^-c^+$) tilting scheme for the monoclinic and orthorhombic structures vary smoothly at this composition. Along the whole compositional range the modes responsible for the out-of-phase tilting of BO_6 octahedra, GM_4^+/R_4^+, remain active, but those associated with the in-phase octahedral tilting, X_3^+/M_3^+, vanish for $x \geq 0.6$, this being associated with the second transition. The symmetry of the new phase will be determined by the remaining primary active mode (with nonzero amplitude) R_4^+. The expected symmetry of the new structure is predicted to be *Imma* with tilting scheme ($a^-a^-c^0$). However, the reorientation of the order parameter from ($aa0$) to (aaa) gives a tilting scheme ($a^-a^-a^-$) and SG $R\overline{3}c$. These two phase transitions seem to be of first order since they can be associated with discontinuities either in the entropy or in the structure.

An additional layered A-site ordering is observed in the rhombohedral structure for low Sr content of the compositional range ($0.6 \leq x \leq 1$): layers of different compositions alternating along the $[111]_p$ direction which is the c axis of the rhombohedral cell ($c_R = 2d_{(111)p}$). In fact, this ordering is due to a rock-salt arrangement of A ions. However, this effect is somewhat local and becomes more and more short range as the Sr content increases.

In many perovskite-like materials, as isotropic pressure is applied (or an internal pressure is induced) transitions to a higher-symmetry phase can occur. A similar trend is observed by raising the temperature. Interestingly, for $x = 1.0$ the three pseudo-cubic cell parameters become very similar, pointing to a transition to a cubic structure which could be obtained by applying pressure, at higher Sr content, or raising the temperature. Therefore, the thermal evolution of the structure of some selected members of the series $La_{2-x}Sr_xCoTiO_6$ ($0 \leq x \leq 1.0$) will be worth investigating. Results in this connection will be published in due course.

Acknowledgements

We thank Ministerio de Economía y Competitividad and Comunidad de Madrid for funding the projects MAT2013-46452-C4-1-R, MAT2013-46452-C4-4-R, PIB2010JP-00181 and S2013/MIT-2753, respectively. Financial support from Universidad San Pablo is also acknowledged. We acknowledge Consejo Superior de Investigaciones Científicas for

financial support and for provision of synchrotron radiation facilities, and we would like to thank beamline staff for assistance in using the BM25-SpLine line. Access to the neutron facilities at the Institut Laue–Langevin is gratefully acknowledged.

References

Adler, S. B. (2004). *Chem. Rev.* **104**, 4791–4844.
Alexei, A. B. & Wei, Y. (2014). *J. Phys. Condens. Matter*, **26**, 163201.
Castro, G. R. (1998). *J. Synchrotron Rad.* **5**, 657–660.
Dachraoui, W., Yang, T., Liu, C., King, G., Hadermann, J., Van Tendeloo, G., Llobet, A. & Greenblatt, M. (2011). *Chem. Mater.* **23**, 2398–2406.
Djurado, E., Boulc'h, F., Dezanneau, G. & Bouvier, P. (2003). *J. Phys. Chem. B*, **107**, 8321–8326.
Dove, M. T. (1997). *Am. Mineral.* **82**, 213–244.
Fergus, J. W. (2006). *J. Power Sources*, **162**, 30–40.
García-Martín, S., Alario-Franco, M. A., Ehrenberg, H., Rodríguez-Carvajal, J. & Amador, U. (2004). *J. Am. Chem. Soc.* **126**, 3587–3596.
Glazer, A. M. (1972). *Acta Cryst.* B**28**, 3384–3392.
Gómez-Pérez, A., Pérez-Flores, J. C., Ritter, C., Boulahya, K., Castro, G. R., García-Alvarado, F. & Amador, U. (2014). *J. Appl. Cryst.* **47**, 745–754.
Hahn, T. (2005). Editor. *International Tables for Crystallography*, Vol. A, *Space-Group Symmetry*, 5th ed. Heidelberg: Springer.
Howard, C. J. & Stokes, H. T. (1998). *Acta Cryst.* B**54**, 782–789.
Howard, C. J. & Zhang, Z. (2004). *Acta Cryst.* B**60**, 249–251.
Ishihara, T. (2009). *Perovskite Oxide for Solid Oxide Fuel Cells*. New York: Springer.
Ishihara, T., Ishikawa, S., Ando, M., Nishiguchi, H. & Takita, Y. (2004). *Solid State Ionics*, **173**, 9–15.
Kennedy, B. J., Howard, C. J. & Chakoumakos, B. C. (1999). *Phys. Rev. B*, **59**, 4023–4027.
Kennedy, B. J., Vogt, T., Martin, C. D., Parise, J. B. & Hriljac, J. A. (2001). *J. Phys. Condens. Matter*, **13**, L925–L930.
Khomchenko, V. A., Troyanchuk, I. O., Többens, D. M., Sikolenko, V. & Paixão, J. A. (2013). *J. Phys. Condens. Matter*, **25**, 135902.
Knight, K. S. (1994). *Solid State Ionics*, **74**, 109–117.
Landau, L. D. & Lifshitz, E. M. (1959). *Statistical Physics*. London: Pergamon.
Le Bail, A., Duroy, H. & Fourquet, J. L. (1988). *Mater. Res. Bull.* **23**, 447–452.
Liu, Z., Han, M.-F. & Miao, W.-T. (2007). *J. Power Sources*, **173**, 837–841.
Magyari-Köpe, B., Vitos, L., Johansson, B. & Kollár, J. (2002). *Phys. Rev. B*, **66**, 092103.
Maupoey, Z., Azcondo, M. T., Amador, U., Kuhn, A., Pérez-Flores, J. C., Romero de Paz, J., Bonanos, N. & García-Alvarado, F. (2012). *J. Mater. Chem.* **22**, 18033.
Maupoey, Z., Azcondo, M. T., Pérez-Flores, J. C., Ritter, C., Boulahya, K., Amador, U. & García-Alvarado, F. (2014). *Dalton Trans.* **43**, 14099.
Mitchell, R. H. (2002). *Perovskite: Modern and Ancient.* Ontario: Almaz Press.
Mountstevens, E. H., Attfield, J. P. & Redfern, S. A. T. (2003). *J. Phys. Condens. Matter*, **15**, 8315–8326.
Orlovskaya, N. & Browning, N. (2004). *Mixed Ionic Electronic Conducting Perovskites for Advanced Energy Systems.* Dordrecht: Springer.
Orobengoa, D., Capillas, C., Aroyo, M. I. & Perez-Mato, J. M. (2009). *J. Appl. Cryst.* **42**, 820–833.
Pagnier, T., Charrier-Cougoulic, I., Ritter, C. & Lucazeau, G. (2000). *Eur. Phys. J. AP*, **9**, 1–9.
Pérez-Flores, J. C., Pérez-Collect, D., García-Martín, S., Ritter, C., Mather, G. C., Canales-Vázquez, J., Gálvez-Sánchez, M., García-Alvarado, F. & Amador, U. (2013). *Chem. Mater.* **25**, 2484–2494.
Pérez-Flores, J. C., Ritter, C., Pérez-Collect, D., Mather, G. C., Canales-Vázquez, J., Gálvez-Sánchez, M., García-Alvarado, F. & Amador, U. (2012). *Int. J. Hydrogen Energy*, **37**, 7242–7251.
Perez-Mato, J. M., Orobengoa, D. & Aroyo, M. I. (2010). *Acta Cryst.* A**66**, 558–590.
Raveau, B. & Seikh, M. (2012). *Dalton Trans.* **40**, 7908.
Rodríguez-Carvajal, J. (1993). *Phys. B Condens. Matter*, **192**, 55–69.
Rubio-Zuazo, J., Collado-Negro, V., Heyman, C., Ferrer, P., da Silva, I., Gallastegui, J. A., Gutiérrez-León, A. & Castro, G. R. (2013). *J. Phys. Conf. Ser.* **425**, 052005.
Shannon, R. D. (1976). *Acta Cryst.* A**32**, 751–767.
Shibasaki, T., Furuya, T., Kuwahara, J., Takahashi, Y., Takahashi, H. & Hashimoto, T. (2005). *J. Therm. Anal. Calorim.* **81**, 575–581.
Sugahara, T. & Ohtaki, M. (2011). *Appl. Phys. Lett.* **99**, 062107.
Sun, X., Wang, S., Wang, Z., Qian, J., Wen, T. & Huang, F. (2009). *J. Power Sources*, **187**, 85–89.
Tolédano, J. C. & Toléadano, P. (1987). *The Landau Theory of Phase Transitions: Application to Structural, Incommensurate, Magnetic, and Liquid Crystal Systems.* London: World Scientific Publishing Company.
Trofimenko, N. (1999). *Solid State Ionics*, **124**, 263–270.
Woodward, P. M. (1997*a*). *Acta Cryst.* B**53**, 32–43.
Woodward, P. M. (1997*b*). *Acta Cryst.* B**53**, 44–66.
Yuste, M., Pérez-Flores, J. C., de Paz, J. R., Azcondo, M. T., García-Alvarado, F. & Amador, U. (2011). *Dalton Trans.* **40**, 7908.
Zhao, J., Ross, N. L., Angel, R. J., Carpenter, M. A., Howard, C. J., Pawlak, D. A. & Lukasiewicz, T. (2009). *J. Phys. Condens. Matter*, **21**, 235403.
Zhou, J. S., Alonso, J. A., Muoñz, A., Fernández-Díaz, M. T. & Goodenough, J. B. (2011). *Phys. Rev. Lett.* **106**, 057201.